

Digital Receiver-based Electronic Intelligence System Configuration for the Detection and Identification of Intrapulse Modulated Radar Signals

A.K. Singh* and K. Subba Rao#

*Defence Electronics Research Laboratory, Hyderabad-500 005, India

#Osmania University, Hyderabad-500 075, India

*E-mail: singh.ak@dlrl.drdo.in

ABSTRACT

An optimum electronic intelligence system configuration incorporating the state of the art technologies and achieving the highest parameter accuracies while processing the complex intrapulse modulated radar signals is presented in this paper. The system is based on the quad digital receiver, a state of the art single board solution for the detection and analysis of modern radar signals. The system consists of base line interferometry configuration for high accuracy direction finding measurement with sector selection based on amplitude direction finding technique. Advanced signal processing algorithms with time frequency analysis are implemented in real time in field programmable gate array to extract all the basic as well as advanced parameters of frequency and phase modulations such as chirp, barker, and poly-phase (Frank, P1-P4) codes in addition to the pulse and continuous wave signals. The intercepted intrapulse modulated signal parameters have been extracted with very high accuracy and sensitivity.

Keywords: Electronic intelligence, quad digital receiver, analog to digital converter, field programmable gate array, electronic warfare, fast Fourier transform, intrapulse

1. INTRODUCTION

The accurate measurement of radar's intrapulse parameters in real time is very essential to determine the characteristic of radar signals, which makes it possible to take counter action against the intended radar¹. First, it is important to determine the primary parameters like frequency, pulse width, amplitude, direction and time of arrival of the radar signals. The analog receiver is capable of measurement of primary parameters but has a limitation of sensitivity, fine accuracy and also resolving time coincidence signals. These limitation being overcome by using the digital receiver, where the parameter extraction happen in frequency domain after fast Fourier transform (FFT) processing. The high sensitivity of the receiver is achieved results of FFT processing gain, accuracy of parameters achieved due to signal processing at higher point FFT and providing solution for simultaneous intercepted signals because of frequency domain analysis. Subsequently, the advanced parameters like pulse modulation, frequency modulation and phase modulation are to be determined using digital receiver. Measurement of these parameters accurately is also important, because it will help to identify two similar radars operating at very close frequency. The digital receiver is a single board solution for the modern day electronic warfare (EW) receivers instead of multiple boards.

2. ELINT SYSTEM CONFIGURATION

The electronic intelligence (ELINT) system based on quad

digital receiver (QDR) presented here will facilitate detection of the radar signal and also provide the range advantage over radar. The ELINT system configuration based on digital receiver is shown in Fig. 1. The system configuration is divided into various sub-systems as per its defined function. The antenna used in the ELINT system employs high gain directional horn antenna to get high sensitivity. The required frequency coverage of the antenna array is 0.5 GHz - 18 GHz, but designing an antenna for such a large bandwidth is very difficult. Hence, the frequency band of 0.5 GHz - 18 GHz is divided into three sub-bands of 0.5 GHz - 2 GHz, 2 GHz - 6 GHz, and 6 GHz - 18 GHz and separate antenna array is designed for each of the sub-bands. Subsequently, the RF frontend i.e. quad superhet receiver is also designed to accept the 12 RF inputs band wise from the different antenna arrays. The input RF signal of 0.5-18 GHz is converted to IF of 750-1250 MHz i.e. 500 MHz bandwidth using superhet receiver frontend. The configured system based on digital receiver, convert the IF signal into digital signal for radar signal parameter measurement based on real time digital signal processing.

The QDR is designed to measure all the basic parameters of the radar like frequency, pulse width (PW), pulse amplitude (PA), time-of-arrival (TOA) and direction of arrival (DOA) of the emitter along with intrapulse modulation present in radar signal². A pulse descriptor word (PDW) is formed, which contain all the measured parameters of radar signal in specific format. The ELINT System intercept various radar operating

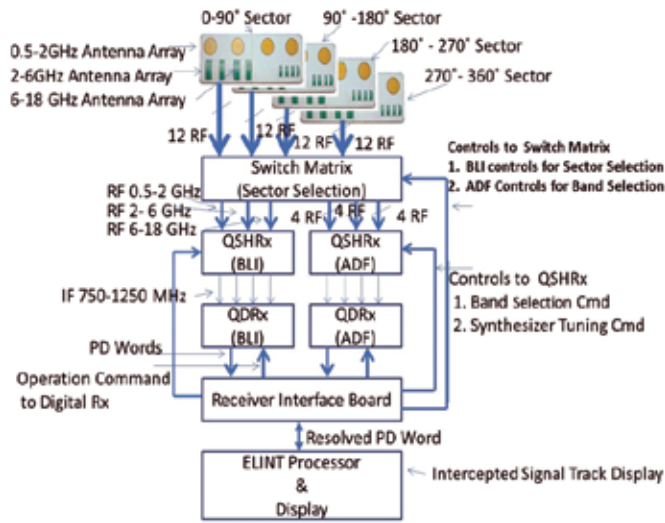


Figure 1. Digital receiver-based ELINT system configuration diagram.

asynchronously, hence measured PDW is interleaved for all the intercepted radar. The interleaved PDW's are interfaced to the main processor where de-interleaving is carried out and radar signal track is displayed. The brief detail of each sub-system is given below.

3. SUB SYSTEM DESCRIPTION

3.1 Antenna Array Sub-System

Antenna array sub-system is designed to intercept the incoming radar signals in the range of 0.5 GHz - 18 GHz and to interface RF Front end receiver. In the present configuration the direction of the arrival (DOA) of the incoming emitter is based on the base line interferometer (BLI) principle and amplitude direction finding is used for resolving the sector information for BLI DF. The four element base line array (BLI Array) provides sector coverage of $\pm 45^\circ$ in azimuth. The phase comparison direction finding system provides DOA accuracy of the order 1° (rms) and it requires coarse information to identify quadrant. The quadrant selection is achieved by four antenna amplitude comparison direction finding system.

Spiral antennas are extremely useful for intercepting any unknown radar signals and play a vital role in modern DF systems in low band i.e. 0.5 GHz - 2 GHz. This spiral antenna also provides broad beam coverage in both the principal planes (Azimuth and Elevation) which leads to easy detection of incoming signals angle of arrival. The BLI array configuration of the spiral antennas is shown in Fig. 2 (a).

Sectorial horn antennas, shown in Fig. 2 (b), are used in 2 GHz - 6 GHz and 6 GHz -18 GHz frequency bands, because of its high gain and small size. The horn antenna provides broad azimuth beam coverage with narrow elevation beam

For BLI phase comparison Direction Finding application, inter-element spacing of the antenna elements is crucial in achieving the required DOA accuracy. The spiral and Sectorial horn antennas in 0.5 GHz - 2 GHz, 2 GHz - 6 GHz, and 6 GHz -18 GHz are being configured into BLI linear arrays with required inter element spacing dictated by the BLI algorithm. All the arrays mounted on a common mounting plate and covered with an overall Radom covering an angular sector of

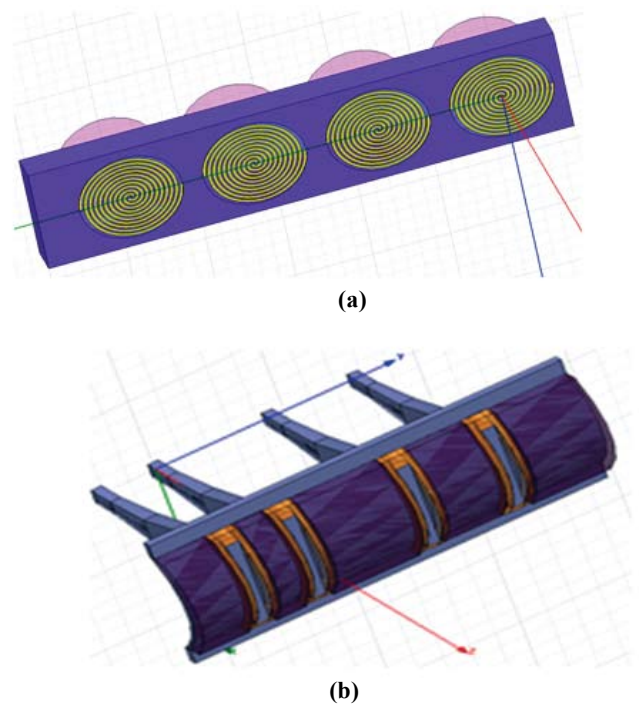


Figure 2. (a) BLI array with spirals antenna and (b) BLI array with sectorial horns antenna.

90° , such 4 arrays are required to cover 360° in Azimuth plane. ELINT system block diagram Fig. 1, shows the coverage of 360° using 4 antenna arrays.

3.2 Antenna Selection Switch Matrix

The antenna head unit consists of 48 directional antenna, 12 antennas in each sector. Each sector is further divided into three bands as explained earlier. The main function of the antenna selection switch matrix is to select one sector and one band of BLI antenna array for fine DOA measurement and one antenna from each sector from the selected band to coarse DF using the amplitude DF technique. This is required because, the ELINT system configuration shown in Fig.1 is based on digital receiver and has very high sensitivity in order of -90 dBm, and hence system will respond for the side lobe and back lobe pick up. The signal pickup from side lobe and back lobe will mislead the operator, hence suitable arrangement has been worked out to eliminate this side and back lobe pick up. Here, antenna selection switch matrix will provide solution for sector resolving, in case of signal pickup from side and back lobes.

3.3 Quad Superhet Rx Frontend

The quad superhet frontend accepts input signals in the range of 0.5 GHz to 18 GHz in split bands of 0.5 GHz - 2 GHz, 2 GHz - 6 GHz and 6 GHz -18 GHz from above mentioned antenna arrays and converts it to IFs of 750 MHz - 1250 MHz bandwidth. To achieve better image rejection and minimum spurious level, three level of mixing arrangement is provided for conversion of RF to IF. The quad superhet receiver is a one of the complex RF technologies, where achieving the gain and phase matching among the four channels was a challenge³. The phase matching of $\pm 25^\circ$ has been achieved after 4 channels RF to IF conversions, which was a difficult task. IF from the

quad superhet receiver is given to quad digital receiver for digitization and parameters extractions of radar signals using the real time signal processing algorithms in FPGAs.

3.4 Quad Digital Receiver

Quad digital receiver is heart of ELINT system. Real time parameters measurement's signal processing algorithms has been implemented in FPGA of QDRx hardware. Quad digital receiver accepts the superhet receiver output of 750 MHz - 1250 MHz and digitizes it using the high speed ADCs and processes the digitized data in FPGAs to extract the radar pulse parameters. The quad digital receiver is an integrated design in a single board for the sampling and processing of four 750 MHz - 1250 MHz radar IF signals. The hardware has been divided into two major sections. They are IF section with clock synthesizer and digital processing PCB.

The IF section is designed as the front end signal conditioning section to accept four input signals in the range of 750 MHz - 1250 MHz. The front end signal conditioning section provides 12 dB effective gain to all four input signals and has an anti-aliasing filter of 750 MHz - 1250 MHz. The gain is required for bringing the signal in to the quantization zone of the ADC using the noise dithering technique and filtering is required for providing rejection to out of band signals, hence avoiding aliasing. Since input to the QDRx is band limited, band pass sampling technique has been used instead of Nyquist Sampling technique. Band pass sampling technique provides advantage of easier hardware design, avoid spectrum wastage and effective data interface with FPGA. Selection of band pass sampling frequency needs to satisfy the following criteria:

$$f_s \geq 2 * BW \quad (1)$$

$$\frac{(2f_c - BW)}{m} \geq f_s \geq \frac{(2f_c + BW)}{m+1} \quad (2)$$

where f_c is centre frequency (1 GHz), BW is bandwidth (500 MHz), f_s is sampling frequency, and m is integer (say 1).

Considering the above two conditions, sampling frequency may be between $1500 \text{ MHz} \geq f_s \geq 1250 \text{ MHz}$. Sampling frequency is selected at the center of the sampling window i.e. 1350 MHz. The sampling frequency of 1350 MHz provides a guard band at both edges because the actual frequency spectrum coverage will be from 675 MHz to 1350 MHz. The synthesized clock of 1.35 GHz has been generated using the reference clock of 10 MHz with phase locked loop (PLL) technique. The phase noise of the clock synthesizer output is maintained below -100 dBc @ 10 KHz, so that the clock jitter can be minimized and higher dynamic range can be achieved by the ADCs.

The quad digital Rx processing PCB is a high speed board design mainly consists of high speed ADCs and Virtex-6 FPGAs as shown in Fig. 3. signal integrity analysis of QDRx has been carried out to ensure the proper impedance matching of high speed traces. The ADC selected for the design is from the Taxes Instruments Part no. ADC10D1500, which provides analog bandwidth of 750 MHz - 1250 MHz @ 1.35 GHz sampling clock. Multiple ADC synchronization feature has been utilized for accurate phase measurement between adjacent channels, which is required for BLI based DF measurement.



Figure 3. Quad digital Rx main board hardware.

Advancements in the FPGAs technology have made possible the implementation of complex DSP algorithms in real time due to the availability of ample resources inside the FPGA. The QDR employs three Virtex-6 FPGAs of millions of gate density for realizing the real time fast Fourier transform (FFT), radar pulse parameters measurement and time-frequency DSP algorithms to extract the intrapulse modulation characteristic like Barker, Frank and Poly-phase (P1-P4).

The signal processing algorithms for intrapulse parameters measurement have been developed in VHDL language and implemented in FPGAs.

3.5 ELINT Processor and Display

The ELINT processor sub-system is designed for generating electronic order of battle (EOB) from measured parameters of radar emitter signals from quad digital receivers. The ESM processor characterizes signals in real time in high density dynamic signal scenario with pulse density in the order of one million pulses per second. The sub-system comprehensively de-interleaves all emitter parameters and identifies by comparing parameters stored in radar libraries. The ELINT processor performs the task of de-interleaving and determines secondary radar parameters such as pulse repetition frequency (PRF), PRF type, scan type and scan period for each emitter and sends emitter file to display.

Display for ELINT system is an EW system operator's console for system operations. The operation of display includes receive intercepted ES data from ES/ELINT payload in near real time, Present the received emitter data in different display formats i.e., Tactical, situational, tabular and map formats.

4. REAL TIME DSP ALGORITHM FOR INTRAPULSE PARAMETERS MEASUREMENT

Real time performance in digital receiver is being achieved by implementing signal processing algorithms in FPGA, where the incoming sampled data and the signal processing speed are matched. In order to be smart to cope up with the large bandwidths, high interleaved signals load, sophisticated advanced algorithms are employed in digital receiver⁴. This section describes the real time measurement algorithms and their implementation in FPGA for frequency,

pulse width, amplitude, time of arrival and DOA of radar signal. The primary parameters of radar signal are based on real time FFT implementation. The major challenges are to get fine resolution in frequency and also in time, because higher points FFT will give good frequency resolution but poor time resolution and vice versa for the lower point FFT. The implemented algorithms explain, how both resolution in time and frequency have been achieved without violating the FFT principle.

4.1 Frequency Estimation of Radar Signal

Frequency of the radar signal is one of the important basic parameters measured by ESM receiver. By comparing the frequency of the pulses received, pulse trains of various radars can be sorted out. To make the jamming and others important actions very effective, better frequency resolution and accuracy are desirable specifications of the receiver. In an electronic warfare scenario, it is required to intercept and resolve multiple radar emitters operating at the same time. So, in order to achieve simultaneous signal resolving capability, FFT is selected as the frequency measurement technique. The input frequency of the signal after normal FFT spectrum analysis is given in Eqn. (3).

$$Measured\ Frequency = \frac{f_s * k}{N} \tag{3}$$

where f_s the sampling frequency and k is the index corresponding to the maximum FFT bin and N is number of points of FFT. Selection of number of points of FFT is a trade-off between the amount of collected data that is processed or computed and the resolution/accuracy that can be achieved in frequency by FFT.

To achieve good frequency accuracy while running the short FFT, interpolation of interbank energy levels in FFT outputs is used. If $K-1$, K and $K+1$ are the locations of previous peak bin, peak bin and next peak bin of the spectrum and α , β , γ are the corresponding amplitudes respectively then, the offset p in frequency bin or interpolated peak location is given in bins by⁵

$$p = \frac{(\alpha - \gamma)}{2 * (\alpha - 2 * \beta + \gamma)} \tag{4}$$

The estimated frequency bin is then measured by

$$Estimated\ Peak\ Bin = k \pm p \tag{5}$$

And estimated frequency can be measured by

$$Estimated\ Frequency = (k \pm p) * \frac{f_s}{N} \tag{6}$$

Using the curve fitting FFT frequency estimation algorithm approach, it is observed that there is huge improvement in frequency resolution and accuracy measurement. In case of 512 points, the frequency measurement accuracies with this approach are less than 0.5 MHz (rms) against 1 MHz (rms) with normal FFT spectrum analysis.

4.2 Pulse Width Estimation

Pulse width is the envelope of the intercepted RF signal. The accurate measurement of pulse width is required to identify the type of radar, whether it is surveillance, tracking or missile homing radar. Accurate PW measurement is achieved with

precise knowledge of leading edge and trailing edge of the pulse. The 512 points FFT provide time resolution of 400 ns, which is not acceptable for the short pulse width signal detection. Overlapping technique has been used to know precisely the Pulse width. The 50 per cent overlapping of input ADC data for FFT will provide 200 ns resolution. Hence, the use of 87.5 per cent overlapping of the input data for FFT has been carried out to achieve 50 ns pulse width resolution. 15 bits has been used to represent pulse width range from 50 ns to 1 ms.

4.3 Time of Arrival Measurement

Time of arrival (TOA) measurement is required to get the PRF of the intercepted radar signals. For TOA calculation, a free running counter of 5 MHz is implemented in FPGA. Whenever there is a signal present, first frame of FFT is used for generating the TOA strobe. At the leading edge of the TOA strobe, the counter value will be registered. The counter value multiplied by the resolution of TOA will yield TOA measurement. The range of TOA varies from 1 ns to 20 ms, which results PRF from 50 Hz to 1 Million pulses per second.

4.4 Pulse Amplitude Measurement

The amplitude of the intercepted radar signal is measured from the FFT spectrum. The data input from the ADC is 10 bit; it is fed to FPGA for 512 points FFT computation. The FFT output i.e. the magnitude spectrum will be 19 bits real and 19 bits imaginary data. The peak value is determined after comparing the values with dynamic threshold. The peak value of real and imaginary FFT output is squared and the square root of the sum of these values is used to find the absolute peak amplitude. This value is used for look up table and mapping the magnitude modulus to the amplitude scale in dBm.

4.5 Direction of Arrival Measurement

Angle of arrival is generally regarded as the best initial sorting parameter because radar cannot change its position immediately, whereas all the other parameters like frequency, PW, amplitude and modulation can be easily changed. BLI is often proposed as a fast and computationally efficient direction finding (DF) technique that provides high accuracy DOA estimates with a small number of receivers, typically 2-4 receivers per quadrant⁶. Principle and its operation of Four antenna BLI technique has been explained Fig. 4.

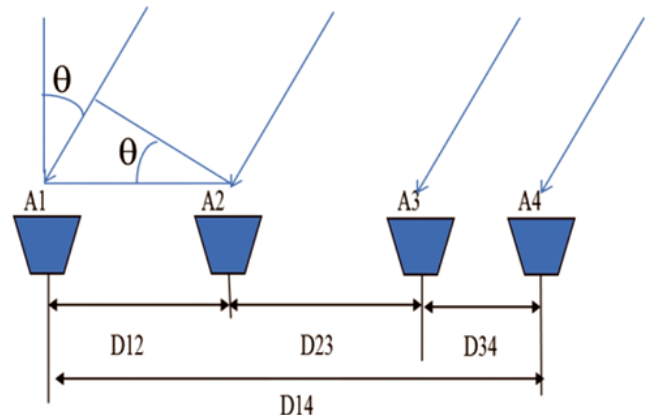


Figure 4. Four antenna phase interferometry-DF.

In Eqn. (7), basic principle of BLI algorithm is explained considering two antennas.

$$\varphi = \frac{(2\pi d \sin \theta)}{\lambda} = \psi + 2\pi m \quad (7)$$

where φ is the true phase delay between two antennas, d is the spacing between the two antennas, λ is the wavelength of the incident signal, θ is the angle of arrival of the signal, ψ is the measured phase delay, and m is an integer.

The Eqn. (7) explained BLI principle and phase difference (φ) between two antennas is measured and DOA (θ) is calculated from the Eqn. (7), because other variables are known or constant. The equation shows that to get more DF accuracy, the distance between two antennas should be large i.e. much more than $\lambda/2$, but it will create phase measurement ambiguity and resultant phase is remainder of modulo 2π . The four antenna BLI configuration for direction of arrival (DOA) is shown in Fig.4, which will provide good accuracy and also help in resolving the phase ambiguity. The spacing's of the antenna array is kept in a ratio of 1:3 shown in Table 1. and using Chinese Remainder Theorem used to resolve the phase ambiguity. The absolute phase difference is obtained by using CORDIC function in each channel at the output of FFT. The four phase difference i.e. phase difference between channel 1 and 2, Channel 2 and 3, Channel 3 and 4 and Channel 1 and 4 are obtained by taking absolute phase difference among the channel respectively.

Table 1. BLI antenna array spacing 1:3 ratio

Freq. (GHz)	D_{12} (mm)	D_{23} (mm)	D_{34} (mm)	Total (mm)	Error	Accuracy
0.5-2	180	540	240	960	4.5°-1.1°	2°
2-6	90	270	120	480	2.2°-0.7°	1°
6-18	30	90	40	160	2.2°-0.7°	1°
Field of view (FOV)					±56°	
Phase margin					±45°	

The 1:3 BLI algorithms for 0.5-2/2-6/6-18GHz band is explained through following equations.

$$D_{12} : D_{23} = 1 : 3 \quad i.e. \quad \psi_{12} : \psi_{23} = 1 : 3$$

$$D_{23} : D_{34} = 9 : 4 \quad i.e. \quad \psi_{23} : \psi_{34} = 9 : 4$$

$$D_{24} : D_{14} = 13 : 16 \quad i.e. \quad \psi_{24} : \psi_{14} = 13 : 16$$

The corresponding phase relations can be written as

$$3 * (\varphi_{12} + 2\pi * m_1) = 1 * (\varphi_{23} + 2\pi * m_2) \quad (8)$$

$$\psi_2 = \varphi_{23} + 2\pi * m_2$$

$$4 * (\varphi_{23} + 2\pi * m_3) = 9 * (\varphi_{34} + 2\pi * m_4) \quad (9)$$

$$4 * \psi_{23} = 9 * \psi_{34}$$

$$16 * (\varphi_{24} + 2\pi * m_5) = 13 * (\varphi_{14} + 2\pi * m_6) \quad (10)$$

$$16 * \psi_{24} = 13 * \psi_{14}$$

here ψ_{14} is the unwrapped phase of longest baseline i.e. between 1 and 4. Solving the equations will result in reduction in the

number of ambiguities (possible values of m_p, m_2 , etc.). It can be seen that the ratio of any two antenna spacing's bears a ratio of mutually prime integers. This feature is used to resolve the phase ambiguity by using the Chinese remainder theorem. The error equation for the BLI based DF is given in Eqn. (11).

$$\delta_0 = \frac{\delta_\varphi \lambda}{(2\pi D \cos \theta)} \quad (11)$$

where δ_0 is the DOA error and δ_φ is the phase measurement error. From the error equation it is seen that the achievable DOA accuracy is better for a longer baseline and also for higher frequency (i.e. smaller λ). This assumes that the phase measurement error is constant throughout the operating bandwidth of the system. Considering these points, it indicates that higher frequencies will give better DOA accuracy than lower frequencies. The resulted set and measured DF from -45° to 45° is resulted in the 1° (rms) DF accuracy for 2 GHz - 6 GHz and 6 GHz - 18 GHz frequency band, which is very much required for effective localisation of scanning emitters⁷.

5. ALGORITHM FOR INTRAPULSE MODULATION EXTRACTION

The real time FFT algorithm implemented in FPGA is suitable for extracting the carrier frequency, amplitude, DOA and also pulse parameters like pulse width, TOA, but it has drawbacks like spectrum correction and spectral leakage, which limits its use phase modulated signals. All Phase FFT is an algorithm to achieve the high accuracy phase measurement without the need for spectrum correcting. With this algorithm, the advanced parameters of the intrapulse modulated radar signal such as Barker, Frank, and Poly-phase (P1, P2, P3 and P4) are analysed.

5.1 Principle of All Phase FFT

The principle of all phase FFT is represented pictorially in the Fig. 5. The input data is firstly windowed by a $(2N-1)$ length window w_c , then every two samples with the space between N intervals (except the middle element $x(0)$) are summed up thus one new N -length data vector $y=[y(0), y(1), \dots, y(N-1)]$ can be formed. Lastly, implementing DFT/FFT on the new vector will generate the outcome of apFFT. The algorithm shown

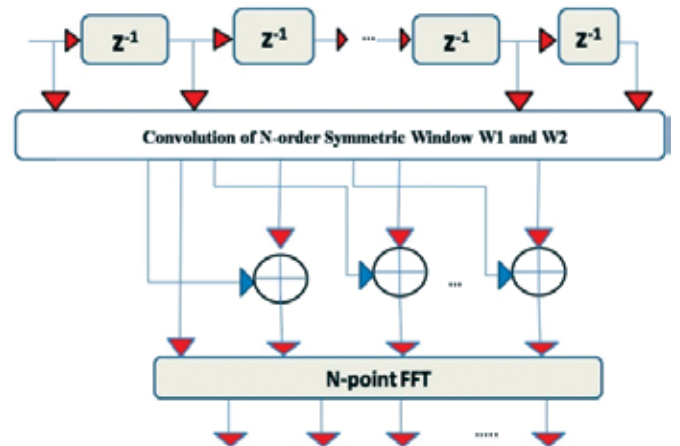


Figure 5. All phase FFT spectrum analysis.

in Fig. 5 is an optimum implementation which makes apFFT convenient to be implemented⁸. wc is named as convolution window, which equals the convolution of one front window $f(n)$ and one reversed back window $b(n)$, i.e.

$$w(n) = f(n) * b(n) \quad (12)$$

5.2 Amplitude Spectrum of APFFT

The amplitude of all phase spectrum is as follows⁹

$$|X_{AP}| = \frac{1}{N} \left| \frac{\sin^2 \pi N \left(\frac{f_0 - k}{f_s - N} \right)}{\sin^2 \pi \left(\frac{f_0 - k}{f_s - N} \right)} \right| \quad (13)$$

This is square of the traditional Fourier transform frequency spectrum amplitude. It can also be noted that all N spectral lines amplitudes obey the same square law, which means that the amplitude ratio of adjacent lines to the peak line decreases more acutely according this square relation. As a result, apFFT possesses a better quality than FFT in inhibiting spectral leakage.

5.3 Phase Spectrum of All Phase FFT

A single-frequency complex exponential sequence $x(n) = e^{(in\omega_0 + \phi_0)}$, $\omega_0 = \beta\Delta\omega$, $\Delta\omega = \frac{2\pi}{N}$, is $N+1 \leq n \leq N-1$, selected as an example to compare the traditional DFT phase spectrum with apDFT phase spectrum. The N -order normalized traditional windowed FFT spectrum $X(k)$ and the N -order normalized dual windowed All phase FFT spectrum $Y(k)$ with can be respectively represented as

$$X(k) = F_g [(k - \beta)\Delta\omega] e^{j\left[\theta_0 - \frac{(N-1)(k-\beta)\Delta\omega}{2}(\beta-k)\pi\right]} \quad (14)$$

$$Y(k) = F_g [(k - \beta)\Delta\omega] e^{j\theta_0} \quad (15)$$

$$k \in [0, N-1]$$

From Eqn. (14) and Eqn. (15), we can infer that having implemented apFFT on the $(2N-1)$ input data, we can directly obtain the central sample's theoretic phase value from the peak spectral line without any additional correcting operations. Thus we say that apFFT possesses the property of 'phase invariant'.

5.4 Simulation Results of All Phase FFT Algorithm

Simulation has been carried out on sinusoidal signal to clearly view the working principle of all phase FFT and to compare it against the no window and windowed FFT. Figure 6 (a) shows the signal plot with no window and the corresponding magnitude and Phase plots using FFT.

Figures 6 (b) and 6(c) shows the signal plot, magnitude and phase plots using FFT with Hamming and Hanning windows respectively. From Figs. 6 (a) - 6(c) we can observe that frequency spectrums of window and no windows are same except for low magnitude in the case of windowed FFT. The phase spectrums of windowed and no windowed FFT are deviating from the actual phase due to non-synchronous sampling. Figure 6(d) shows the phase and magnitude plots for the all phase FFT. From Fig. 6(d) we can clearly say that with the all phase FFT the phase of the signal can be identified clearly as the frequency and also the phase is invariant for nearby indexes also and is completely unambiguous. This particular property of all phase FFT is used for the extracting the phase changes in the digital phase modulations.

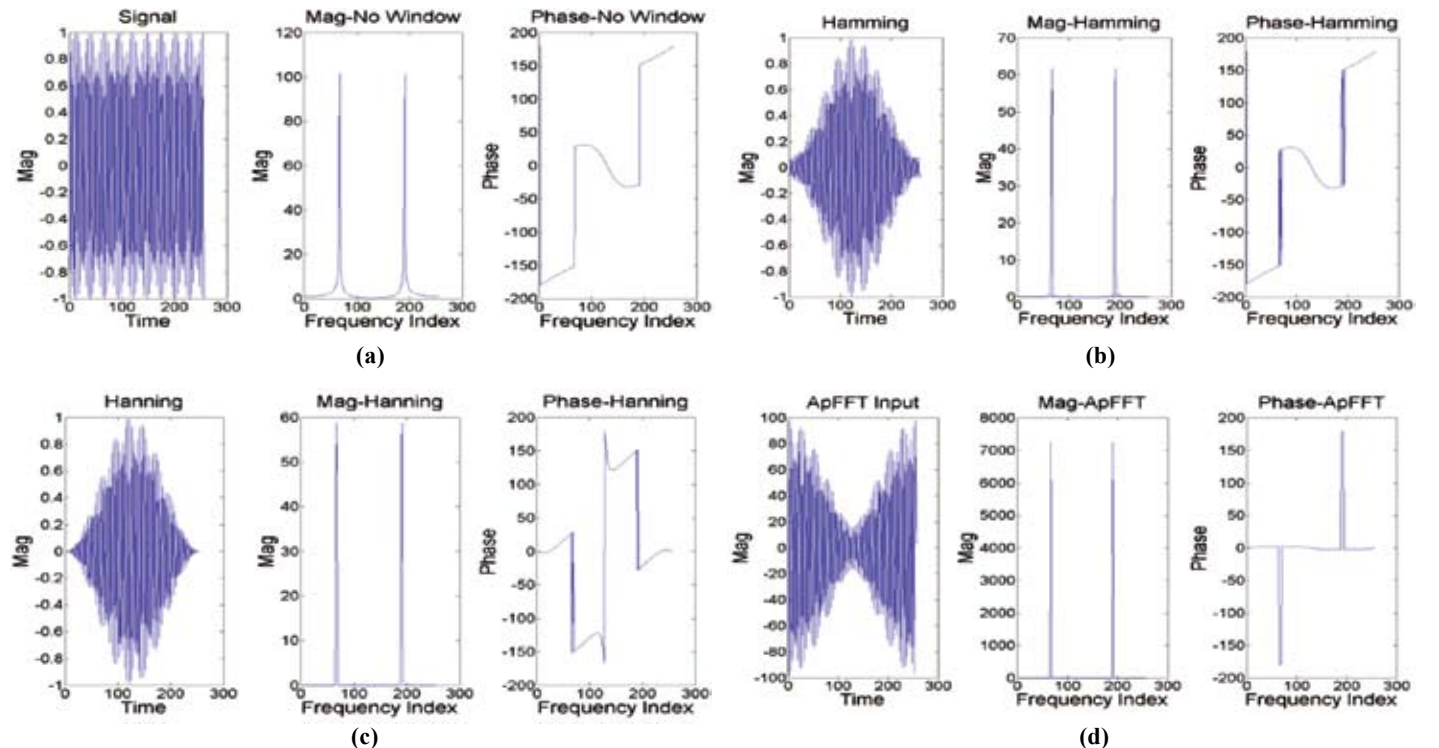


Figure 6. Magnitude and phase spectrums: (a) No window, (b) Hamming window, (c) Hanning window, and (d) All phase FFT.

5.6 Implementation of apFFT in Digital Receiver

After the phase collection from the all phase FFT the phase information within the 256 bin is obtained. This phase is again unwrapped to get the actual phase. Whenever there is a phase change happens within the samples under consideration the phase from the central bin will deviate from the actual one. From the information obtained through the previous frame and next frame the phase change is calculated. If there is no phase change is present then the signal is considered as a pulse modulated signal. Similarly if the frequency from the successive frames differs then the signal will be classified as a Frequency modulated signal. If the signal is having phase modulation then the phase change pattern is obtained. For testing the effectiveness of the algorithm against the detection of various intrapulse modulation signals, the signal is being generated from the arbitrary waveform generator since it is an ideal instrument to generate complex real world signals¹⁰. The signal from the AWG is being digitized by the High Speed ADC and is processed in the FPGA of the digital receiver to extract the various basic and advanced parameters of the intrapulse modulated signals. The results are monitored using the chip scope pro tool of FPGA. The types of the signals and the intrapulse modulation that can be obtained with the above algorithm are shown in Table 2.

Table 2. Effectiveness of algorithm

Parameter	Extracted signal parameters
Type of signals	Chirp, Barker, Frank, P1-P4
Parameters of chirp signals	Centre frequency, chirp bandwidth, chirp rate
Phase modulation parameters	Sub code duration, phase pattern, type of phase code

Table 3 shows the output phase of a Barker and Frank code that are being extracted with the apFFT algorithm. It is also observed that the phase error is within $\pm 5^\circ$, which is sufficient to extract all the polyphase modulations.

Table 3. Extracted phase for Barker and Frank code

Type of signal	Actual phase pattern	Achieved phase pattern
Barker 7	+ + + - - + -	0 0 0 180 180 0 180
	0 0 0 0 0 0 0	0 0 0 0 0
Frank 4	0 90 180 270	0 89 180 270
	0 180 0 180	0 180 0 179
	0 270 180 90	0 267 180 87

6. CONCLUSION

The digital receiver based system is the modern day solution for the interception, detection and analysis of basic as well as advanced radars in real time with high parameter accuracies and sensitivity. The proposed digital Rx based ELINT system configuration meets the operational requirements of modern ELINT system and can also be customised to meet ELINT system requirements of tri-services.

REFERENCES

1. Pace, P. E. Detecting and classifying LPI radar. Ed. 2nd, Artech House, 2008.
2. James, Tsui. Special design topics in wideband digital receivers. Artech House Inc., Norwood, Massachusetts, 2010.
3. Pekau, H. & Haslett, J.W. A comparison of analog front end architectures for digital receivers. *In the Proceedings of the IEEE CCECE/CCGEI*, Saskatoon, May 2005.
4. Barkan, Uri & Yehuda, Shuki. Trends in radar and electronic warfare technologies and their influence on the electromagnetic spectrum evolution. *In the Proceedings of the IEEE 27th Convention of Electrical and Electronics Engineers*, Israel, 2012, pp. 5.
5. Quinn, B.G. Estimating frequency by interpolation using fourier coefficients. *IEEE Trans. Signal Proc.*, 1994, **42**, 1264-1268.
6. Peter, Q.C. Ly; Stephen, D.E.; Douglas, A.G. & Joy, Li. Unambiguous AOA estimation using SODA interferometry for electronic surveillance. *In the Proceedings of the IEEE 7th Sensor Array Multi channel signal processing work shop (SAM)*, 2012, pp.277-280.
7. Hatem, H. & Kutluyil, D. Passive localization of scanning emitters. *IEEE Trans. Aerospace Electro. Sys.*, 2010, **46**,(2), 941- 951.
8. Huang, Xiangdong & Wang, Zhaohua. Phase difference correcting spectrum method based on all-phase spectrum analysis. *J. Electro. Info. Technol.*, 2008, **30**(2), 293-297.
9. Guo, Jing; Li, Nan; Zhou, Zhou; Yi, Wei; Xu, Xin & Wang, Yinan. A novel digital demodulation method for MFEIT based on APFFT. *In the Proceedings of the IEEE International Conference on Intelligent System Design and Engineering Application*, 2010, doi:10.1109/ISDEA.2010.239
10. Hoehne, Beate. Digital up conversion vs IQ modulation using a wideband arbitrary waveform generator. *In the Proceedings of the IEEE Auto Test Conference*, 2012, pp. 299-302.

CONTRIBUTORS



Mr A.K. Singh completed ME in digital system (ECE) from Osmania University in 2003. Currently he is working as a Scientist ‘F’ at DLRL, Hyderabad and leading a team working on design of real time digital receiver. His area of interest includes : High speed board design, time-frequency signal processing, and EW receiver design.



Dr K Subba Rao has Graduated from S.V. University, Tirupati in India. He obtained his Master’s and PhD from Osmania University, Hyderabad, India. His current interests include signal processing for Radar signal, spread spectrum applications and bio medical signal processing.